

Mini Review

## Research Progress of Metal Oxide as Cathode Materials for Hydrogen Evolution

Hao Xu\*, Fuchao Li, Zihan Li, Qunjun Liu, Bokai Li, Longfei Xu, Guosheng He

Jiangsu Xinhai Power Generation Co., Ltd. Lianyungang, Jiangsu 222012, P. R. China.

\*E-mail: [189210033@stu.just.edu.cn](mailto:189210033@stu.just.edu.cn)

Received: 10 October 2022 / Accepted: 13 November 2022 / Published: 30 November 2022

---

This review provides an overview of the latest research on metal oxide-based hydrogen evolution reaction (HER) catalysts, describes the synthesis of composite compounds or heterostructures based on metal oxides, classifies metal oxide-based hydrogen evolution catalysts by metal element type, and discusses the advantages and limitations of each catalyst. From noble metal oxides to transition metal oxides, to rare earth metal oxides, and finally to perovskite-type oxides, are discussed in detail. Further good electrocatalytic activity and durability of metal oxide-based heterostructures are obtained due to the synergistic catalytic effect of the heterostructures, which can modulate the electronic structure of the active site. Finally, an outlook on the future development of hydrogen evolution catalysts is given by summarizing the shortcomings and challenges of existing hydrogen evolution catalysts.

---

**Keywords:** Hydrogen evolution reaction; Metal oxides; Heterostructures; Catalysts; Electrocatalytic activity

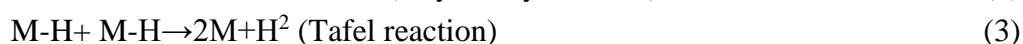
### 1. INTRODUCTION

With the depletion of fossil energy sources, the energy crisis is gradually approaching, and the search for alternative new energy sources has become an urgent task. Hydrogen energy has great advantages such as high calorific value, friendly to the environment, and can be widely used in fuel cells in the future, therefore, hydrogen energy is generally considered as an important alternative to fossil energy sources [1-3]. To use hydrogen for energy conversion, we must first consider the production of hydrogen, and there are many means to produce hydrogen, among which hydrogen production using electrolytic water method is a sustainable, safe and green way to produce hydrogen [4].

Hydrogen production by electrolysis of water has been receiving much attention, and this method has several advantages [5, 6]: (i) hydrogen production by using the low valley electricity of the power grid can fully save and utilize energy, (ii) electrolysis of water is safe and environmentally friendly, raw materials are easily available, and the purity of hydrogen produced is high, (iii) hydrogen production by

electrolysis of water can regulate the rate of hydrogen production by adjusting the tank voltage. By comparing the cathodic hydrogen evolution state under acidic and alkaline conditions, it can be found that there is enough  $H^+$  to react on the electrode surface under acidic conditions to facilitate the electrolysis of water, but the hydrogen evolution materials will be less stable due to corrosion, and the acidic conditions often involve proton exchange membranes, which increases the cost, so it is difficult to carry out large-scale electrolytic hydrogen production under acidic media in industry [7]. Currently, hydrogen production by electrolysis of water in alkaline solutions is a more mature method for hydrogen production in industry, and the hydrogen evolution cathodes tend to be more stable in alkaline solutions, making it easier to control the overall hydrogen evolution rate. However, energy consumption problems, high overpotential of the cathode, catalyst activity and durability have been affecting the alkaline electrolytic water hydrogen production industry.

The catalytic activity of hydrogen evolution catalysts in acidic media is closely related to the adsorption energy of hydrogen atoms, and researchers have summarized a "volcano plot" relationship for this purpose [8, 9]. However, the HER process in alkaline media is somewhat more complex, as it also involves three reaction mechanisms (Eqs. (1)-(3), with the catalyst denoted by M) [10] and hydrogen reduction via two possible combinations of Volmer-Heyrovsky or Volmer-Tafel pathways. Unlike the HER process in acidic solutions, the H-O-H bond in water needs to be broken in the Volmer step of alkaline solutions before the hydrogen atoms adsorbed by the catalyst (M-H) can be generated, since there is no sufficient  $H^+$  in alkaline solutions, and this process affects the catalyst activity and makes the kinetics of hydrogen evolution in alkaline solutions slow. Further, the Volmer process in alkaline solution also involves factors such as the adsorption energy of water on the surface of the hydrogen evolution catalyst, the affinity between  $OH^-$  and the cathode surface, etc. When the binding energy of the catalyst to water increases, it leads to faster adsorption between the catalyst and water, which results in a faster Volmer step. However, when too much  $OH^-$  covers the catalyst surface and poisons the active site, it leads to a decrease in catalyst activity [11]. It can be seen that the development of cathodic catalysts in alkaline media cannot simply follow the "volcano plot" rule, and the catalytic activity of the catalyst is influenced by three factors: (i) a good ability to dissociate the adsorbed water on the surface, (ii) a good ability to bind newborn hydrogen atoms, (iii) the hydroxide ion should have a low affinity at the active site on the catalyst surface. And these factors affect the catalyst activity, stability and energy consumption issues.



Precious metals have excellent catalytic activity as hydrogen evolution catalysts, but considering their high cost, they cannot be used for large-scale industrial applications, and people have to look for other materials for substitution. At this stage, a variety of non-precious metal-based HER catalysts, especially nickel-based alloys, have been prepared, but it is still difficult to achieve catalytic activity and stability comparable to that of Pt and other noble metals [12].

Recent studies have found that metal oxides, especially transition metal oxides, including noble metal oxides, rare-earth metal oxides and perovskite-structured oxide, can be used as cathode hydrogen evolution materials to achieve a continuous and stable HER process at a low overpotential, and they also

have promising applications in energy conversion and storage, showing great advantages. However, using metal oxides alone as catalysts for hydrogen evolution is again lacking in catalytic activity, and researchers have found that heterostructured hydrogen evolution materials with both high stability and strong catalytic activity can be obtained by constructing several structures such as metal/metal oxide, metal oxide/metal oxide, metal oxide/nonmetal compounds, or coupling metal oxides with highly conductive carbon materials [13, 14]. At present, there are few studies on the mechanism of HER on metal oxides, and there is great scope to further improve the catalytic activity of metal oxide-based catalysts for HER. This review will analyze the advantages and disadvantages of metal oxide-based hydrogen evolution catalysts in the context of recent research, and will focus on the hydrogen evolution effects of various types of metal oxide composite compounds or heterostructures, and will provide an outlook on the future development of metal oxide catalysts.

## 2. NOBLE METAL OXIDE MATERIALS FOR HYDROGEN EVOLUTION

Due to the high catalytic activity and stability of noble metals in their state of simple substance, their oxides have been less studied as catalysts. The application of noble metal oxides in hydrogen evolution catalysts is mainly focused on two elements, ruthenium and iridium, both of which are transition metals.

Lee et al. [15] synthesized RuO<sub>2</sub> nanoparticles containing crystalline water by heating and stirring an aqueous RuCl<sub>3</sub> solution at 95°C for 18 h. TEM tests showed that they had a low crystallinity. The RuO<sub>2</sub> containing crystalline water was loaded on nickel foam to form RuO<sub>2</sub>/Ni electrode, and the polarization curves were tested in 1 M KOH solution, and it was found that the catalytic performance of RuO<sub>2</sub> containing crystalline water was better than that of RuO<sub>2</sub> in the state without crystalline water under the same conditions, and even higher than that of commercially available Pt/C catalysts. The hydrogen evolution overpotential was only 60 mV at a current density of 10 mA/cm<sup>2</sup>, and the overpotential did not increase significantly after a 50-h test at this current density, reflecting the excellent catalytic activity and stability of this material. However, RuO<sub>2</sub> containing crystalline water tends to decompose into anhydrous crystalline RuO<sub>2</sub> at higher temperatures.

RuO<sub>2</sub> does not have high catalytic activity at high overpotential, Cheng et al. [16] prepared RuO<sub>2</sub>/Ni-P/Ni composite electrode on Ni substrate using pulsed electrodeposition method, and found by linear scanning voltammetry (LSV) and electrochemical impedance (EIS) tests in 1.0 M NaOH solution that the presence of RuO<sub>2</sub> reduced the charge transfer resistance of the composite at low overpotential, while the presence of Ni-P reduced the charge transfer resistance at high potential, with an overpotential of 70 mV for HER at a current density of 10 mA/cm<sup>2</sup> for the RuO<sub>2</sub>/Ni-P/Ni electrode (Fig. 1a). However, it has a Tafel slope of 77 mV/dec, which is higher than that of Ni-P/Ni electrode (Fig. 1b).

Zhang et al. [17] synthesized RuO<sub>2</sub>-NiO nanorod arrays in situ on nickel foam substrates using a hydrothermal method, and XPS tests showed that the Ru atomic percentage was only 2.15%, but the catalytic activity of the RuO<sub>2</sub>-NiO/Ni electrode was high (6 M NaOH,  $\eta = 100$  mV, current density 100 mA/cm<sup>2</sup>), surpassing the RuO<sub>2</sub>/Ni electrode with a relatively high proportion of Ru atoms [18] and the overpotential only slightly increased after 60 h electrolysis test.

Iridium oxide electrodes are mostly used as oxygen evolution electrodes for electrolytic water [19, 20] and for HER processes also prefer acidic media. Vidales et al. [21] investigated the hydrogen evolution performance of Ni-Mo-Ir oxides under acidic conditions, firstly, electrode materials with different molar ratios were prepared using the thermal decomposition method, and it was found by testing that as the surface roughness increased with the increase of Ir content in the Ni-Mo-oxide coating, and the hydrogen evolution current at constant potential also increased. Normalized for the surface area effect, the estimation showed that the intrinsic catalytic activity (specific activity) leveled off after the Ir content reached 40%. The potential of the Ni-Mo-Ir oxide did not change significantly after high current density and long-time electrolysis tests with a pure Ni electrode as a control, while the overpotential of the Ni electrode kept increasing. After electrolysis, the electrocatalytic activity of metallic Ni was found to be reduced to about half of the initial activity by Tafel test, while the activity of Ni-Mo-Ir oxide coating could be maintained at more than 85% of the initial value, which fully reflects the good stability of Ni-Mo-Ir oxide. However, when metal ion impurities are present in the electrolyte, it is easy to deactivate this electrode.

For other noble metal oxides, Ibrahim et al. [22] prepared PdO/TiO<sub>2</sub> nanocomposites using a two-step process of solvothermal and high-temperature calcination. Coated on a glassy carbon electrode (GCE), a current density of 10 mA/cm<sup>2</sup> was achieved at an overpotential of 195 mV in a strong alkali solution of 4 M NaOH, which is not very far from the Pt/C catalyst ( $\eta_{10}$  = 135 mV), indicating the excellent stability and durability of the material at high overpotentials.

From the above study, by combining noble metal oxides with non-precious metals and metal oxides, it is possible to reduce the cost and ensure the catalytic activity and stability of the electrodes.

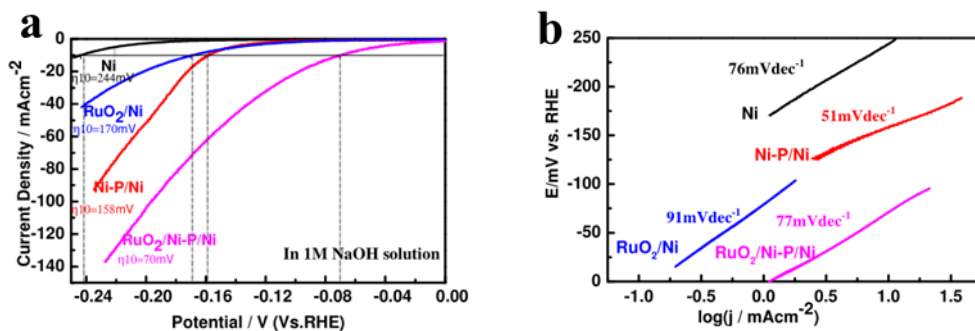


**Figure 1.** (a) LSV and (b) Tafel plots of Ni, Ni-P/Ni, RuO<sub>2</sub>/Ni and RuO<sub>2</sub>/Ni-P/Ni catalysts in the 1.0 M NaOH electrolyte at a sweep rate of 10 mV s<sup>-1</sup>. Reproduced with permission [16]. Copyright 2017, Elsevier.

### 3. TRANSITION METAL OXIDE HYDROGEN EVOLUTION MATERIALS OTHER THAN NOBLE METAL OXIDES

Although noble transition metals such as Ru, Ir and their oxides possess excellent catalytic properties and stability, they are expensive and relatively scarce, making them difficult for large-scale applications. It has been found that some non-precious transition metals exhibit excellent HER catalytic activity, By increasing the degree of transition metal oxide/metal hybridization and creating

heterogeneous structures, it is possible to increase the electrical conductivity and expose more active sites, resulting in highly active and stable catalysts for hydrogen evolution [14, 23, 24]. The metal oxide hydrogen evolution materials of the three transition series classified by the position of the transition metals in the periodic table of elements are described below.

### 3.1. First-row transition metal oxide hydrogen evolution materials

The first-row transition metal elements are Sc~Ni, which are located in the 4th cycle of the periodic table. Except for the rare earth element Sc, the other metal elements are relatively inexpensive compared to the precious metals and have the prospect of being used as alternative materials to the noble metal catalysts.

#### 3.1.1. Ni, Co metal oxide hydrogen evolution materials

Among the first-row transition metal elements, Ni and Co exhibit better HER catalytic activity and are the most widely used; recently, some literature reported that the oxide nanoscale materials of two metals, Ni and Co, have good HER catalytic activity.

The metal Ni is widely used in alkaline HER processes, but the prolonged use of nickel as an alkaline HER catalyst increases the overpotential of nickel substantially. Some researchers have found by scanning electron microscopy and X-ray diffraction that the decay of nickel-metal activity is due to the formation of nickel hydride, which has a low density of electronic states in the Fermi energy level of the d-band [25, 26], and the presence of nickel hydride hinders the hydrogen desorption ability, which leads to an increase in the hydrogen evolution overpotential [25]. It has also been suggested that the OH<sup>-</sup> adsorbed on the pure nickel surface may occupy the sites of H atoms, thus slowing down the ensuing Volmer process and hindering H adsorption [12].

In order to improve the catalytic stability of Ni, NiO has been studied and efforts have been made to improve the catalytic activity of NiO-containing catalysts. Gong et al. [12] prepared a NiO/Ni-CNT heterostructured catalytic electrode coupled to carbon nanotubes with a HER current density of 10 mA/cm<sup>2</sup> at 100 mV overpotential in 1 M KOH solution. The catalytic electrode was first produced by low-temperature hydrolysis of nickel salts to nickel hydroxide [Ni(OH)<sub>2</sub>/ox-CNT] on the sidewalls of mildly oxidized carbon nanotubes (CNTs), followed by low-pressure annealing at 300 °C in an argon atmosphere. Ni/CNT and NiO/CNT were prepared by a similar method for comparison, and the hydrogen evolution overpotential of the NiO/Ni-CNT electrode was found to be much lower than that of NiO/CNT and lower than that of Ni/CNT by measuring the polarization curves. Through the mechanism level, the OH<sup>-</sup> from H<sub>2</sub>O cleavage preferentially attaches to the NiO surface, and the Ni surface will promote the adsorption of H, thus accelerating the Volmer process.

Yan et al. [27] proposed a crystalline/amorphous Ni/NiO core/shell nanosheet, where Ni/NiO was first generated on the surface of nickel foam substrate by hydrothermal method and annealing, and then the described material was obtained after treatment at an appropriate temperature under a hydrogen atmosphere, and the HER current density of 10 mA/cm<sup>2</sup> in 1 M KOH corresponded to an overpotential of 145 mV. The stability test at 9000 s showed that the current density decreased from 8.3 mA/cm<sup>2</sup> to

5.8 mA/cm<sup>2</sup> at 150 mV overpotential, which shows that this material is only suitable for application at low overpotential and has a certain lack of catalytic activity and stability. Similarly, Liu et al. [28] prepared porous Ni/NiO nanosheet arrays on nickel foam with the help of a non-contact Al reduction method with an onset overpotential close to zero in 1 M NaOH, and the Ni/NiO arrays could provide current densities of 20, 50 and 100 mA/cm<sup>2</sup> at overpotentials of 46, 92 and 137 mV, respectively. By comparison, the structures of the Ni/NiO nanosheets prepared in both papers are similar, with low crystallinity of NiO and both presenting as core-shells, but the Ni/NiO nanosheet arrays prepared by a non-contact Al reduction method are more uniform and ordered.

Zhang et al. [29] prepared NiO nanorods with a large number of O vacancies in situ on carbon fiber paper by cation exchange method using ZnO nanorod arrays as a template. The total number of vacancies can be regulated by controlling the cation exchange temperature, and it was found that the NiO nanorods corresponding to a moderate amount of oxygen vacancies at 585 °C had the best HER catalytic activity, showing an overpotential of about 110 mV at a current density of 10 mA/cm<sup>2</sup> in 1 M KOH solution. At higher overpotential states, the NiO nanorods show even higher current densities than the industrially used Pt/C catalysts. Stability testing of this electrode by the chrono-current method revealed that it showed only a slight current decay of 6% after 10 h of continuous testing. Mott-Schottky tests and DFT calculations indicated that the higher conductivity of NiO with the introduction of O vacancies was the main reason for its improved HER catalytic activity and stability.

Lu et al. [30] proposed a unique Li<sub>x</sub>NiO/Ni heterostructure fabricated on graphene or nickel foam, the heterostructure was produced by the reaction between molten Li and NiO with an overpotential of only 36 mV at a current density of 10 mA/cm<sup>2</sup> in 1 M KOH solution, which is comparable to the effect of Pt/C electrode, and concluded that the Li<sub>x</sub>NiO and Ni effective synergy between them accelerates the Volmer step (Fig. 2).

In addition to Ni oxides, metal Co oxides have also been studied for the preparation of HER catalysts. Ling et al. [14] also prepared Ni, Zn double-doped CoO nanorods with a large number of O vacancies using ZnO nanorods as a template using cation exchange method. It was found that the Ni, Zn double-doped CoO nanorods synthesized with 11% Ni and 2% Zn dopant concentrations had the best catalytic performance, corresponding to overpotentials of 53 and 79 mV at current densities of 10 and 20 mA/cm<sup>2</sup> in 1 M KOH solution, respectively; tested at a current density of 10 mA/cm<sup>2</sup> for 24 h, the overpotentials were essentially unchanged and showed good stability. At a current density of 100 mA/cm<sup>2</sup>, the overpotential of Ni and Zn double-doped CoO nanorod electrode was even lower than that of Pt/C catalyst. The DFT calculations and conductivity tests showed that the double-doped CoO nanorods have the best free energy of hydrogen adsorption surface  $\Delta G_{H^*}$  and higher turnover frequency (TOF) values.

Yan et al. [31] prepared three-dimensional Co/Co<sub>3</sub>O<sub>4</sub> core/shell nanosheets on nickel foam corresponding to a crystalline Co core and an amorphous Co<sub>3</sub>O<sub>4</sub> shell, respectively, which required an overpotential of only 129 mV in 1 M KOH to achieve a current density of 20 mA/cm<sup>2</sup>, which is better than the cobalt-cobalt oxide/N carbon hybrid (CoO<sub>x</sub>@CN) bifunctional material (hydrogen evolution at the cathode and oxygen evolution at the anode) with better catalytic activity for hydrogen evolution [32], and a CoO<sub>x</sub>@CN electrode in 1 M KOH requires an overpotential of 232 mV to achieve a current density of 10 mA/cm<sup>2</sup>. Liu et al. [33] prepared Co/CoO nanowire arrays directly on nickel foam using

hydrothermal and special Al thermal reduction methods, and Co nanoparticles were embedded in CoO arrays to form a three-dimensional layered structure, and the overpotential was only 167 mV at a current density of 100 mA/cm<sup>2</sup> in 1 M NaOH solution, which was only 95 mV larger than that of the Pt/C electrode at the same current density. After 24 h, the corresponding current densities of 20 and 50 mA/cm<sup>2</sup> did not change, indicating that the stability of the electrode material is excellent.

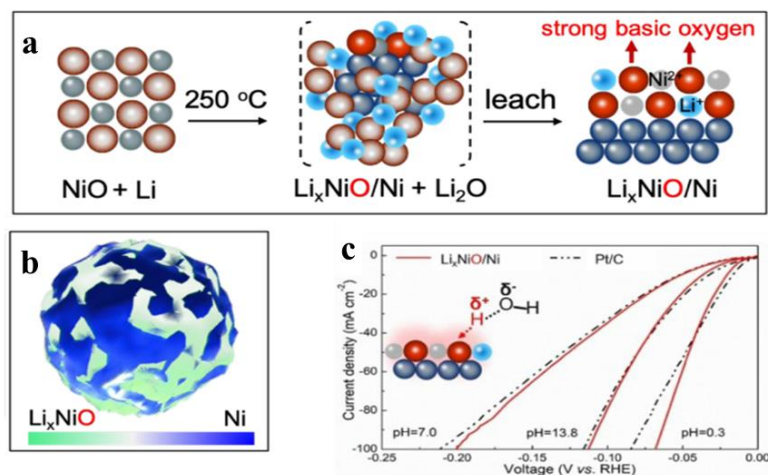


**Figure 2.** (a) Illustration of the molten Li mediated synthesis process and generation of strong basic oxygen species. (b) Synthesis of nanoscale Li<sub>x</sub>NiO/Ni heterostructures on graphene. (c) Linear sweep voltammograms (LSV) curves at 5 mV/s in three different media. Reproduced with permission [30]. Copyright 2020, ACS Publications.

### 3.1.2. First-row transition metal oxide hydrogen evolution materials other than Ni and Co

In addition to Ni and Co, other metal oxides of the first-row transition metals are also used in HER catalysis, but most of the prepared hydrogen precipitating materials are coordinated with other elements. Saha et al. [34] prepared MnO<sub>2</sub>/NiO@Ni heterostructured electrodes in situ on nickel foam using hydrothermal method. The corresponding overpotential was 230 mV at a current density of 23.8 mA/cm<sup>2</sup> in 1 M KOH, but with the rise of electrolyte pH, the corresponding overpotential rose rapidly, and in 6 M KOH, the corresponding overpotential at a current density of 11.2 mA/cm<sup>2</sup> even reached 4.1 V. It can be seen that the electrode material is not suitable for use in strongly alkaline solutions.

Ti oxides have also been used in HER catalysis, Feng et al. [35] electrodeposited ZnO nanorods on carbon fiber (CFs) substrates as templates to first generate Co nanosheet nanotubes (NSNTs) by electrodeposition and chemical reaction, and then immersed in titanium salts to synthesize TiO<sub>2</sub> NDs/Co NSNTs-CFs containing TiO<sub>2</sub> nanodots (NDs), in which TiO<sub>2</sub> NDs belong to the amorphous phase. Polarization tests revealed that the electrode had only 106 mV overpotential in 1 M KOH at a current density of 10 mA/cm<sup>2</sup>, and the overpotential was found to remain essentially unchanged after 30 h of testing at this current density by the chrono-current method. The results fully demonstrate the excellent catalytic activity and stability of the TiO<sub>2</sub> NDs/Co NSNTs-CFs electrode. The hydrogen adsorption free energy  $\Delta G_{H^*}$  of TiO<sub>2</sub>/Co hybrids at 0 V and 0.2 V overpotential was calculated by DFT to be 0.18 eV

and 0.02 eV, respectively, which is closer to 0 eV with respect to both Co and TiO<sub>2</sub>, which enables more desirable adsorption and desorption of H on the catalyst surface and thus promotes HER (Fig. 3). Previously, a researcher loaded Pt nanoparticles on TiO<sub>2</sub> (Pt-TiO<sub>2</sub>) to prepare nitrogen-doped reduced graphene oxide (N-rGO)-based nanocomposite (Pt-TiO<sub>2</sub>-N-rGO) [36], which exhibited a maximum current density of 126 mA/cm<sup>2</sup> at an overpotential of 300 mV in 0.1 M H<sub>2</sub>SO<sub>4</sub>, but the expensive price of Pt metal and the effect on the material under alkaline conditions the hydrogen evolution effect is not yet known, making it difficult to perform large-scale applications.

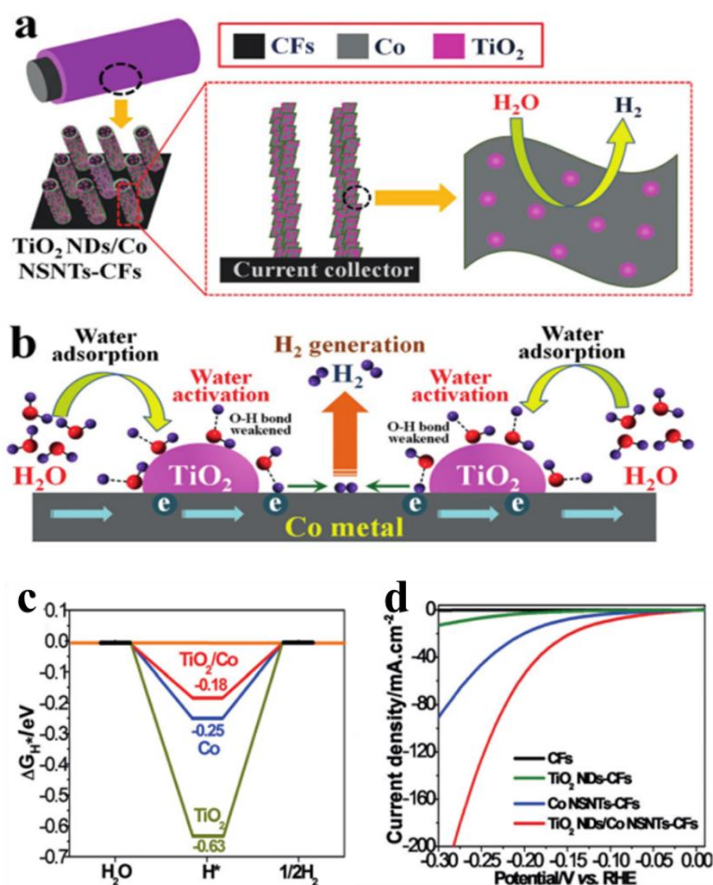


**Figure 3.** (a) Schematic illustration of the microstructure of TiO<sub>2</sub> NDs/Co NSNTs-CFs. (b) Schematic illustration of water adsorption, water activation, and hydrogen generation processes. (c) DFT calculation of kinetic energy barrier profiles of H formation on TiO<sub>2</sub>, Co and TiO<sub>2</sub>/Co at overpotential of 0 V. (d) Polarization curves of TiO<sub>2</sub> NDs/Co NSNTs-CFs, Co NSNTs-CFs, TiO<sub>2</sub> NDs-CFs and CFs. Reproduced with permission [35]. Copyright 2017, Wiley Online Library.

Involving the doping of noble metals, Nong et al. [37] used Ru-doped SrTiO<sub>3</sub> to make SrTi<sub>1-x</sub>Ru<sub>x</sub>O<sub>3</sub> precursors, which were then etched by HCl to obtain Ru-doped TiO<sub>2</sub> (TiO<sub>2</sub>:Ru), where part of the Ti in TiO<sub>2</sub> accepts electrons from Ru and turns into Ti<sup>3+</sup>. The number of oxygen vacancies in the TiO<sub>2</sub>:Ru system was further increased by further reduction of TiO<sub>2</sub>:Ru by non-contact Al to obtain R-TiO<sub>2</sub>:Ru, while 5% Ru doping was found to be the most suitable. The overpotential of R-TiO<sub>2</sub>:Ru (5%) in 0.1 M KOH was 150 mV at 10 mA/cm<sup>2</sup>, which was 41 higher than Pt/C mV.

In addition, Narayanan et al. [38] prepared  $\text{Cr}_2\text{O}_3$  powder using hydrothermal method and coated the powder onto different substrates for experiments, where the Tafel slope of Pt/ $\text{Cr}_2\text{O}_3$  electrode with Pt as substrate was 50% lower than that of Pt electrode in 0.1 M NaOH.

Rao et al. [39] prepared VO in situ on nickel foam (NF) substrate using hydrothermal method and then vulcanized it using  $\text{H}_2\text{S}/\text{N}_2$  (1/9 by volume) to obtain VO-S/NF electrode with overpotentials of 248 and 165 mV for unvulcanized VO/NF and vulcanized VO-S/NF, respectively, when provided with  $10 \text{ mA}/\text{cm}^2$  current density in 1 M KOH, suggesting that the vulcanization process may expose more active sites and thus improve the catalytic activity.

It can be found that the first-row transition metal oxides are widely used in HER catalysts, and the catalytic effects are all very obvious. Considered at the level of replacing precious metals, not only does it save some cost, but also the catalytic effect is not much different from that of precious metals, and some catalyst materials even surpass the performance of precious metal catalysts at high current densities.

### 3.2. Second-row transition metal oxide hydrogen evolution materials

The second-row transition metal elements are Zr~Pd, which are located in the 5th cycle of the periodic table. Except for Ru, Rh and Pd, which are precious metals, and Tc, which is a man-made rare element, which is less applied due to the cost, Zr, Nb and Mo are widely studied. Among them, Mo is widely used in HER catalysts and is often alloyed with other metal elements. As for the hydrogen evolution catalysts with oxides of the second transition metal elements, there are few reports on oxides of other elements except Mo.

Metal Mo is often alloyed with Ni and other metals in an alloy phase for catalytic hydrogen production under alkaline electrolytic conditions, and the practical application of such alloys is often limited by poor stability, i.e., dissolution of metal Mo in alkaline solutions under intermittent electrolytic conditions [13]. In contrast,  $\text{MoO}_2$  has a high chemical stability and metal-like conductivity [40] and a surface hydrogen adsorption free energy  $\Delta G_{\text{H}^*}$  of +0.15 eV, which is very favorable as a catalytic material for hydrogen evolution [41]. Among the many  $\text{MoO}_2$ -based heterostructured catalysts, several materials have more promising catalytic activities, as detailed in Table 1.

On the whole,  $\text{MoO}_2$ -based hydrogen evolution materials are similar to the first transition system metal oxide-based heterostructured materials mentioned above.  $\text{MoO}_2$ -based heterostructured electrodes are mostly prepared by more than two-step processes, which involve mainly hydrothermal synthesis, high-temperature calcination (annealing) reduction, vapor deposition, electrodeposition, acid etching, etc.  $\text{MoO}_2$ -based heterostructured catalysts in alkaline media generally promote the cleavage of water molecules, which accelerates the Volmer step and thus the HER process.

**Table 1.** Electrochemical catalytic performance of MoO<sub>2</sub>-based hydrogen evolution catalysts.

Catalysts	Electrolytes	Substrates	Overpotential and		Load	References
			corresponding current density	Tafel slope		
Ru–MoO <sub>2</sub>	0.5 M H <sub>2</sub> SO <sub>4</sub>	GCE	55 mV@10 mA/cm <sup>2</sup>	44 mV/dec	0.285 mg/cm <sup>2</sup>	[40]
	1 M KOH		29mV@10 mA/cm <sup>2</sup>	31mV/dec		
NFL MoO <sub>2</sub> /NF	1 M KOH	Ni Foam	55 mV@10 mA/cm <sup>2</sup>	66 mV/dec	4.5 mg/cm <sup>2</sup>	[42]
MoS <sub>2</sub> /MoO <sub>2</sub>	0.5 M H <sub>2</sub> SO <sub>4</sub>	ACC	300 mV@85 mA/cm <sup>2</sup>	35.6 mV/dec	0.3 mg/cm <sup>2</sup>	[43]
MoO <sub>2</sub> /MoSe <sub>2</sub>	0.5 M H <sub>2</sub> SO <sub>4</sub>	ACC	181 mV@10 mA/cm <sup>2</sup>	49.1 mV/dec	0.13 mg/cm <sup>2</sup>	[44]
MoNi <sub>4</sub> /MoO <sub>2</sub> @Ni	1 M KOH	Ni Foam	15 mV@10 mA/cm <sup>2</sup>	30 mV/dec	43.4 mg/cm <sup>2</sup>	[45]
MoO <sub>2</sub> /α-Mo <sub>2</sub> C	1 M KOH	GCE	100 mV@10 mA/cm <sup>2</sup>	50mV/dec	N/A	[46]
	0.5 M H <sub>2</sub> SO <sub>4</sub>		152 mV@10 mA/cm <sup>2</sup>	65mV/dec		
MoSe <sub>2</sub> /MoO <sub>2</sub>	0.5 M H <sub>2</sub> SO <sub>4</sub>	Mo foil	142 mV@10 mA/cm <sup>2</sup>	48.9mV/dec	N/A	[47]
MoO <sub>2</sub> P <sub>x</sub> NSs/P-MWCNTs	0.5 M H <sub>2</sub> SO <sub>4</sub>	GCE	57 mV@10 mA/cm <sup>2</sup>	45mV/dec	0.35 mg/cm <sup>2</sup>	[48]
Pt Cs/MoO <sub>2</sub> NSs-L	0.5 M H <sub>2</sub> SO <sub>4</sub>	N/A	47 mV@10 mA/cm <sup>2</sup>	32.6mV/dec	0.5 wt% Pt	[49]
MoO <sub>2</sub> -Ni NWs/NF	1 M KOH	Ni Foam	47 mV@10 mA/cm <sup>2</sup>	36.6 mV/dec	2.2 mg/cm <sup>2</sup>	[50]
MoO <sub>2</sub> @CoMo	0.5 M H <sub>2</sub> SO <sub>4</sub>	CP	76 mV@-50 mA/cm <sup>2</sup>	38.1~50mV/dec	N/A	[41]

Notes: NFL means nanoflower-like; MWCNTs means multiwalled carbon nanotubes; NSs means nanosheets.

In addition to molybdenum oxide-based electrodes, niobium oxides (Nb<sub>2</sub>O<sub>5</sub>) are often used as photoelectrode catalysts in conjunction with other compounds. The poor activity of Nb<sub>2</sub>O<sub>5</sub> for HER catalysis in electrolytic water is mainly attributed to its poor conductivity and more dense structure [51]. Li et al. [52] compared the Nb<sub>2</sub>O<sub>5</sub> and Nb<sub>2</sub>N (Nb<sub>2</sub>O<sub>5</sub> annealed in ammonia atmosphere) HER properties, and the measured Tafel slope of 146 mV/dec for Nb<sub>2</sub>O<sub>5</sub> in 0.5 M H<sub>2</sub>SO<sub>4</sub> was much larger than that of the Nb<sub>2</sub>N electrode (92 mV/dec). Similar to Nb<sub>2</sub>O<sub>5</sub>, zirconium oxide (ZrO<sub>2</sub>) is often used as a photocatalytic electrode, and the material has high chemical durability [48], in addition, ZrO<sub>2</sub> is more widely used as a good hydrogen storage material [53], but ZrO<sub>2</sub> has been little studied in the electrolysis of aqueous HER processes. Gao et al. [54] prepared Ni-S-Co/ZrO<sub>2</sub> composites by electrodeposition, and the overpotential was 145 mV at 100 mA/cm<sup>2</sup> current density in a NaOH solution with a mass fraction of 28%, which decreased by 50 mV compared with that without the addition of ZrO<sub>2</sub>, and from SEM

images and potential step tests, it can be known that the addition of  $\text{ZrO}_2$  increased the true surface area and roughness of the electrode, thus improving the catalytic performance.

It can be seen that only molybdenum oxides, among the second-row transition metal elements, are very widely used in the field of hydrogen evolution catalysts, and are a very promising class of materials for use in HER catalysts, similar to its effect in the state of simple substance. Molybdenum oxides improve stability and can effectively synergize with other substances in the catalyst to accelerate the HER process.

### 3.3. Third-row transition metal oxide hydrogen evolution materials

The third-row transition metals are Hf~Pt, which are located in the 6th cycle of the periodic table. In addition to the three noble metals Os, Ir, and Pt, there are also four elements Hf, Ta, W, and Re. The application of oxides of these four elements in HER catalysts is less frequent than that of the first-row and second-row transition metal oxides, which is related to their price, the amount of mineral deposits in the earth's crust, and catalytic performance.

Recently, Demir et al. [48] prepared a  $\text{Ru}^0/\text{HfO}_2$  (2.00% wt. Ru) catalytic material for hydrogen evolution using sodium borohydride reduction of Ru(III) ions impregnated on  $\text{HfO}_2$ , which was coated onto a glassy carbon electrode and tested in 0.5 M  $\text{H}_2\text{SO}_4$  and found to exhibit a hydrogen evolution overpotential of 75 mV at 10  $\text{mA}/\text{cm}^2$ , showing good catalytic activity. However, compared with  $\text{Ru}^0/\text{ZrO}_2$  (41 mV@10  $\text{mA}/\text{cm}^2$ ) and  $\text{Ru}^0/\text{TiO}_2$  (65 mV@10  $\text{mA}/\text{cm}^2$ ) prepared by the same method,  $\text{Ru}^0/\text{HfO}_2$  is somewhat lacking in catalytic effect. In addition, the turnover frequency (TOF) is an important way to consider the catalytic activity of the electrodes, taking the TOF value of Pt electrode at 0.0 V as a benchmark, while  $\text{Ru}^0/\text{HfO}_2$  requires an overpotential of 52 mV to achieve the same TOF value, which is higher than  $\text{Ru}^0/\text{ZrO}_2$  (38 mV) and  $\text{Ru}^0/\text{TiO}_2$  (43 mV) electrodes. The reason for the difference in catalytic activity of these three materials may also partly depend on their specific surface areas ( $\text{HfO}_2$ -6  $\text{m}^2/\text{g}$ ,  $\text{ZrO}_2$ -32  $\text{m}^2/\text{g}$ ,  $\text{TiO}_2$ -63  $\text{m}^2/\text{g}$ ).

Tantalum oxides have low catalytic activity on electrolytic water HER and are commonly used as photosensitive catalysts, so they have not been studied much in the direction of electrochemical hydrogen production. Although the most stable form of tantalum oxide is the pentavalent state, there are likewise multiple oxidation states of the unsaturated form of  $\text{TaO}_x$  [55]. Awaludin et al. [56] attempted the electrochemical reduction of  $\text{Ta}_2\text{O}_5$ , a method that converts  $\text{Ta}^{5+}$  to  $\text{Ta}^{<5+}$ , first using electrodeposition methods on a glassy carbon electrode (GCE) to prepare a  $\text{TaO}_x/\text{GC}$  electrode and then immersed in 2 M  $\text{H}_2\text{SO}_4$  solution at a rate of 20 mV/s for 30 reduction potential scans from 0 to -0.7 V. Then, the test in 0.5 M  $\text{H}_2\text{SO}_4$  solution revealed a minimum overpotential of 236 mV at 1  $\text{mA}/\text{cm}^2$ , which obviously enhanced the HER activity. This is followed by up to 6000 reduction scans, which gradually decrease the hydrogen evolution overpotential of the electrode, and after 6000 scans possibly  $\text{TaO}_x$  undergoes detachment, leading to the beginning of performance degradation. Overall, the HER catalytic performance of the  $\text{TaO}_x/\text{GC}$  electrode is poor, but this method of improving the catalytic activity opens a new path for the development of metal oxide-based catalysts.

Tungsten-based compounds have many applications in the field of electrochemical hydrogen production, where W elements are often combined with C, P, and N. The resulting catalysts have HER

activity even close to that of Pt electrodes [57]. Recently, Yang et al. [58] prepared WS<sub>2</sub> films on carbon fiber paper (CFP) by pyrolysis, and then prepared WO<sub>3</sub>-2H<sub>2</sub>O/WS<sub>2</sub> hybrid catalysts by simple anodic treatment of WS<sub>2</sub> films in 0.5 M H<sub>2</sub>SO<sub>4</sub> solution by cyclic voltammetry, and found by testing that with a pyrolysis temperature of 600°C and 6 cycles of anodic oxidation treatment The electrode catalytic performance was the best, showing an overpotential of 152 mV at a current density of 100 mA/cm<sup>2</sup>. The results show that pure WO<sub>3</sub>-2H<sub>2</sub>O is inert in HER and hydrogen migrates from the WO<sub>3</sub>-2H<sub>2</sub>O nanoplate to the active sites (defects and edges) of WS<sub>2</sub>, fully demonstrating the synergistic interaction between WO<sub>3</sub>-2H<sub>2</sub>O and WS<sub>2</sub> to enhance the catalytic activity. Moreover, in the same time frame, Shibli et al. [59] deposited Ni-P-WO<sub>3</sub> coatings on mild steel (MS) by a three-step process of hydrothermal, annealing and chemical plating with a Tafel slope of 108 mV/dec in 32% NaOH, exhibiting superior catalytic activity to that of the Ni-P alloy.

Although rhenium (Re) is not included in the list of 17 rare earth elements, rhenium is a truly rare element. Recently, some researchers have investigated the HER catalytic behavior of rhenium oxides. Kim et al. [60] prepared ReO<sub>3</sub> nanoparticles (reductant is methanol) and ReO<sub>3</sub> nanosheets (reductant is ethanol) on carbon fiber paper (CFP) using hydrothermal method, and then introduced oxygen vacancies by argon plasma treatment of 480s to form ReO<sub>3</sub> NP/CFP-480s and ReO<sub>3</sub> NS/CFP-480s electrodes. The overpotential decreased from 157 mV and 178 mV to 138 mV and 145 mV, respectively, in 0.5 M H<sub>2</sub>SO<sub>4</sub> at a current density of 10 mA/cm<sup>2</sup>, and was able to remain stable under 20 h of electrolysis. The DFT calculations showed that ReO<sub>3</sub> has a high density of states at the Fermi energy level, and the introduction of oxygen vacancies brought  $\Delta G_{H}^*$  closer to zero, which improved the catalytic activity.

Soon after, Feng et al. [61] used graphene-polyimide (G-PI) as a substrate to heat a homemade ReO<sub>3</sub> precursor in a tube furnace with argon (Ar) as a protective atmosphere at 450 °C. The ReO<sub>2</sub> vapor could then be deposited on the G-PI substrate to form vertical ReO<sub>2</sub> arrays, and then the formed ReS<sub>2</sub>/ReO<sub>2</sub> heterostructured materials were prepared by vulcanizing the formed ReO<sub>2</sub> arrays in another tube furnace. The overpotential is 150 mV at a current density of 10 mA/cm<sup>2</sup> in 0.5 M H<sub>2</sub>SO<sub>4</sub>. DFT calculations show that the heterostructure of ReS<sub>2</sub>/ReO<sub>2</sub>, with a work function almost close to the energy level of the H<sup>+</sup>/H<sup>2</sup> potential, is more favorable for the reductive evolution of hydrogen.

In summary, the oxides of the third-row transition metal elements have great promise in hydrogen evolution catalysis, especially the oxides of two elements, tungsten and rhenium, have shown good results and will be gradually used more and more in HER catalysis in the future.

#### 4. RARE EARTH METAL OXIDE HYDROGEN<sub>2</sub> EVOLUTION MATERIALS

Rare earth compounds have attracted increasing attention in recent years and are considered as potential electrocatalytic materials with stability and acid-base properties due to their unique electronic structure in the 4f electronic layer and thus excellent chemical and optical properties [62]. There are 17 rare earth elements, lanthanides and scandium and yttrium, and at present, rare earth oxides are still more sparsely studied in catalysts than other transition metal oxides.

Cerium oxides (CeO<sub>2</sub>) in the lanthanide family have received increasing attention for their excellent properties in applications such as fuel cells, oxygen storage capacitors, sensors and other

biological fields [63], and recently, CeO<sub>2</sub> has been increasingly investigated for its excellent stability in HER catalysis, such as Ni-CeO<sub>2</sub> [64], Ni-S/CeO<sub>2</sub> [65], Ni-P-CeO<sub>2</sub> [66], CeO<sub>2</sub>-Fe<sub>2</sub>O<sub>3</sub>-Ni-P [67], CeO<sub>2</sub>-RuO<sub>2</sub>-Ni-P [68, 69], CeO<sub>2</sub> particles in the electrode can expand the specific surface area of the electrode and also create a synergistic effect with Ni and other substances to enhance HER catalytic activity. Weng et al. [70] presented a mixed metal/metal oxide nanoparticle material (Ni/CeO<sub>2</sub>-CNT) grown on carbon nanotubes (CNT) with a catalytic current density of 32 mA/cm<sup>2</sup> for Ni/CeO<sub>2</sub>-CNT in 1 M KOH solution at an overpotential of 150 mV, and the current density was maintained at about 30 mA/cm<sup>2</sup> for 10 h of continuous electrolysis. The DFT calculations showed that the Ni/CeO<sub>2</sub> interface lowered the energy barrier for OH-H bond cleavage and promoted the dissociation of water molecules to form hydrogen atoms, and the lowered hydrogen bond energy (HBE) accelerated the desorption of H\* and thus promoted the production of H<sub>2</sub> (Fig. 4).

In addition to CeO<sub>2</sub>, recently Liu et al. [71] prepared samarium oxide modified Sm<sub>2</sub>O<sub>3</sub>-Ni-Co/NF on nickel foam using electrodeposition method, where Sm<sub>2</sub>O<sub>3</sub>-Ni-Co vertical nanosheets on the surface of nickel foam were intertwined to show a honeycomb shape. An overpotential of 276 mV in a 1.0 M KOH electrolyte was required to achieve a current density of 10 mA/cm<sup>2</sup>. It can be seen that the materials under the electrodeposition preparation conditions did not exhibit excellent catalytic effects, which may be related to the nature of the materials themselves and also the homogeneity of the plated surface.

The effect of yttrium (Y) as a light rare earth element and its oxide on the electrochemical properties of hydrogen precipitating materials has been rarely mentioned. Earlier, Yi et al. [72] prepared Ni-Co-Y<sub>2</sub>O<sub>3</sub> composite plating on titanium substrate using electrodeposition and tested in 0.50 M Na<sub>2</sub>SO<sub>4</sub> + 0.10 M H<sub>2</sub>SO<sub>4</sub> solution and found that the presence of Y<sub>2</sub>O<sub>3</sub> promoted HER catalysis and the hydrogen evolution potential at 10 mA/cm<sup>2</sup> current density compared to Ni-Co alloy shifted in the positive direction by about 100 mV. Similarly, Voskanyan et al. [73] later electrodeposited a ZrO<sub>2</sub>-CeO<sub>2</sub>-Y<sub>2</sub>O<sub>3</sub> composite layer on a titanium substrate with a minimum Tafel slope of 30 mV/dec in a 1.0 M KOH electrolyte, and the higher catalytic performance could be a result of synergistic catalysis between the multi-metal oxides. Since there are not many HER catalytic materials with heterogeneous structures of yttrium oxides, there are not many reports on the detailed mechanism of their catalytic promotion.

He et al. [74] attempted to prepare Ni-Co-Gd<sub>2</sub>O<sub>3</sub> composite layer containing rare-earth gadolinium oxide (Gd<sub>2</sub>O<sub>3</sub>) using electrodeposition, and electrochemical tests revealed that in a 0.5 M Na<sub>2</sub>SO<sub>4</sub> + 0.1 M H<sub>2</sub>SO<sub>4</sub> solution, the hydrogen evolution potential of the Ni-Co-Gd<sub>2</sub>O<sub>3</sub> composite plating at a current density of 9 mA/cm<sup>2</sup> positively shifted about 130 mV (compared to the Ni-Co plating), which indicates that the embedded Gd<sub>2</sub>O<sub>3</sub> particles enhanced the catalytic activity of the original Ni-Co plating only.

In a previously mentioned paper [22], in addition to PdO/TiO<sub>2</sub> nanocomposites, Eu<sub>2</sub>O<sub>3</sub>/TiO<sub>2</sub> nanocomposites were prepared by the same method, also in 4 M NaOH strong base solution Eu<sub>2</sub>O<sub>3</sub>/TiO<sub>2</sub> had a Tafel slope of 135 mV/dec, which is larger than the PdO/TiO<sub>2</sub> material (125 mV/dec) is larger than that of PdO/TiO<sub>2</sub> material (125 mV/dec). The reason for this is mainly the higher specific surface area of PdO/TiO<sub>2</sub> and the superior conductivity of Pd compared to Eu. Although Eu<sub>2</sub>O<sub>3</sub>/TiO<sub>2</sub> is not as active as PdO/TiO<sub>2</sub> material in terms of catalytic activity, it shows comparable stability in long time electrolysis tests at high overpotential.

It can be found that the metal oxide-based HER catalytic materials of rare earth elements have high stability and electrical conductivity in both acidic and basic media. The synergistic catalytic effect occurs when rare earth metal oxides are used as co-catalysts together with other metals or non-metals to form heterogeneous structures. However, at this stage, the research on rare-earth oxides in HER catalysis is still relatively small and does not fully demonstrate the excellent performance of rare-earth metal oxides, but it is not a bad choice to replace precious metal materials.

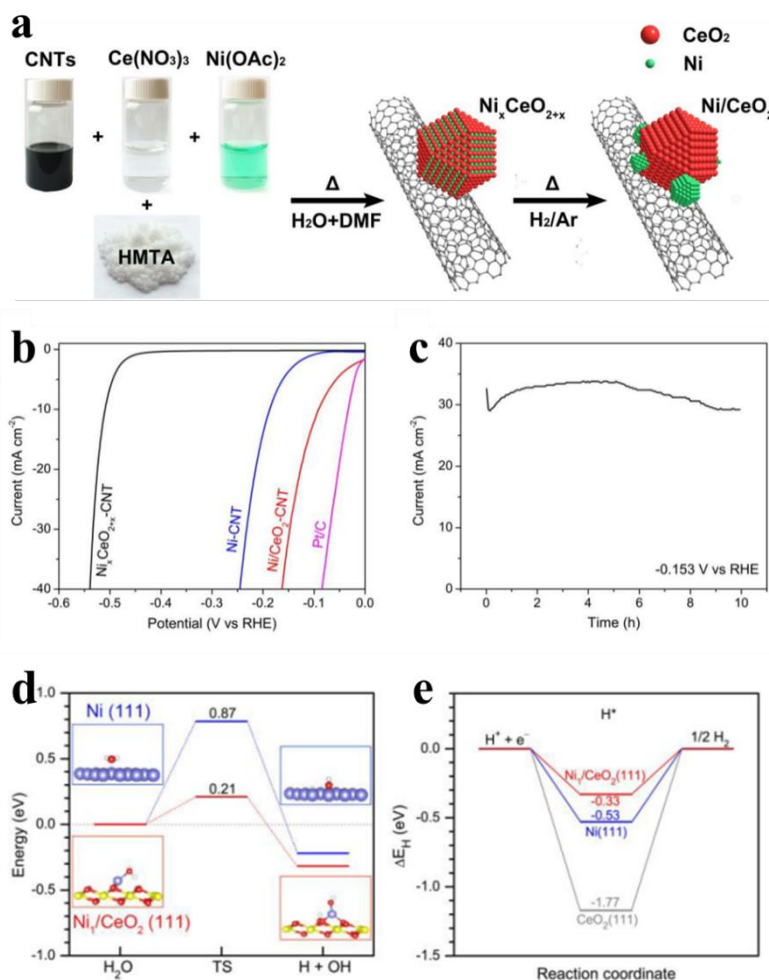


**Figure 4.** (a) Schematic synthesis strategy for creating nanoscale Ni/CeO<sub>2</sub> interfaces on CNTs. (b) Polarization curves of Ni/CeO<sub>2</sub>-CNT, Ni<sub>x</sub>CeO<sub>2+x</sub>-CNT, Ni-CNT and commercial Pt/C in 1 M KOH solution. (c) Amperometric i-t curve of the Ni/CeO<sub>2</sub>-CNT at a constant overpotential of 0.153 V. (d) DFT calculated reaction energy diagram of water dissociation for Ni<sub>1</sub>/CeO<sub>2</sub>(111) and Ni(111). (e) DFT calculated HBE for Ni<sub>1</sub>/CeO<sub>2</sub>(111), Ni(111), and CeO<sub>2</sub>(111) systems. Reproduced with permission [70]. Copyright 2015, ACS Publications.

## 5. PEROVSKITE-TYPE OXIDE HYDROGEN EVOLUTION MATERIALS

Perovskite-type oxides, with the general formula ABO<sub>3</sub> (A = rare earth or alkaline earth metal cation, B = transition metal ion), are emerging as novel and effective catalysts for oxygen reduction (ORR) and oxygen evolution (OER) reactions as an alternative to noble metals [75-77]. Inspired by this, some researchers have started to apply perovskite-type oxides to HER catalysis by doping the A site or

B site in the  $ABO_3$  structure while generating oxygen vacancies, thus changing the physical and chemical properties of perovskite.

Xu et al. [78] prepared  $Pr_x(Ba_{0.5}Sr_{0.5})_{1-x}Co_{0.8}Fe_{0.2}O_{3-\delta}$  perovskite-type oxides using the sol-gel method, and the electrode had good catalytic performance when  $x = 0.5$ , with hydrogen evolution over a current density of  $10 \text{ mA/cm}^2$  in a  $1.0 \text{ M KOH}$  electrolyte with a Tafel slope of  $45 \text{ mV/dec}$ . Rarely, the electrode can maintain continuous hydrogen production for 25 h at a high current density of  $50 \text{ mA/cm}^2$  without significant performance degradation. This result indicates that doping a certain amount of Pr in the A site of perovskite can significantly improve the HER performance.

Zhang et al. [79] also prepared  $SrCo_{0.7}Fe_{0.25}Mo_{0.05}O_{3-\delta}$  (SCFM0.05) using the sol-gel method, which corresponded to an overpotential of  $323 \text{ mV}$  at a current density of  $10 \text{ mA/cm}^2$  in  $1.0 \text{ M KOH}$  with a Tafel slope of  $94 \text{ mV/dec}$ . The doping of Mo element in the perovskite-type B site enhanced the catalytic activity and stability of HER to some extent, but the actual effect was not as ideal as expected and was far from that of Pt/C electrode, which might be related to the incompatibility between the highest percentage of Sr element and other elements leading to the evolution of metal Sr.

Sun et al. [80] prepared an orthogonal double perovskite structure material  $PrBaCo_2O_{5+\delta}$  by simply varying the annealing temperature on the basis of the sol-gel method, and it was found experimentally that the annealing temperature of  $1100 \text{ }^\circ\text{C}$  was beneficial to enhance the electrocatalytic activity and stability of the material towards HER. Electrochemical tests were performed using a rotating disc electrode system at  $1600 \text{ rpm}$  with an overpotential of  $245 \text{ mV}$  at a current density of  $10 \text{ mA/cm}^2$  in an Ar-saturated (dissolved oxygen removed)  $0.1 \text{ M KOH}$  electrolyte. The considerable correlation was calculated using DFT simulations between the p-band center of O and the HER overpotential, and this material with the highest O p-band center at  $1100 \text{ }^\circ\text{C}$  showed the best HER activity. This shows that the crystal structure of the perovskite-type oxide can be adjusted by changing the annealing temperature to achieve the desired catalytic effect.

Sugawara et al. [81] prepared a  $SrRuO_3$ /CNT composite containing the noble metal Ru to enhance the electrical conductivity of the material using carbon nanotubes (CNT). The hydrogen evolution overpotential at a current density of  $10 \text{ mA/cm}^2$  in  $1.0 \text{ M KOH}$  was about  $109 \text{ mV}$  and the Tafel slope was about  $45 \text{ mV/dec}$ , which was better than some previous perovskite-type HER catalysts prepared by other researchers. Despite the presence of Ru precious metal elements in this material, the above catalytic effect can be achieved with only  $0.018 \text{ mg/cm}^2$  of perovskite-type oxide on the electrode surface.

Zhu et al. [82] synthesized a  $Sr_2RuO_4$  material with both perovskite and rock salt layer structures using a solid-phase reaction method, consisting of alternating perovskite layer  $SrRuO_3$  and rock salt layer  $SrO$ . In  $1 \text{ M KOH}$  solution, the overpotential is only  $61 \text{ mV}$  at  $10 \text{ mA/cm}^2$  (Fig. 5a). In addition, the Tafel slope of the electrode was measured to be  $51 \text{ mV/dec}$  (Fig. 5b), which is by far the most catalytically active oxide material for HER, comparable to Pt/C electrode. Through theoretical calculations, it is found that the cleaved  $SrO$  end-group surface of the rock salt layer promotes the decomposition of water, while the active apical oxygen site in perovskite layer can promote the adsorption and escape of hydrogen, which fully reflects the unique synergistic effect between this layered material (Fig. 5c, Fig. 5d).

To investigate the effect of different perovskite-type oxides on catalytic HER processes, Guan et al. [83] introduced the A-site ionic electronegativity (AIE) of perovskite-type oxides as a predictor for screening highly active hydrogen evolution reactions, and simulations showed that the peak HER activity at moderate AIE values of about 2.33 was associated with the optimal electronic state at the active B site. The double perovskite ( $\text{Gd}_{0.5}\text{La}_{0.5}\text{BaCO}_2\text{O}_{5.5+\delta}$ ) prepared according to the predicted results was tested for HER in 1.0 M KOH at room temperature, and the current density at 0.24 V overpotential could reach  $338 \text{ mA/cm}^2$  with a corresponding Tafel slope of  $27.6 \text{ mV/dec}$ , and had a high catalytic level of turnover frequency (TOF) value of  $22.9/\text{s}$ , the performance of this hydrogen evolution catalyst is even better than most of the catalysts in the market, such as Pt/C catalysts.

Perovskite-type oxides with their ability to dope multiple elements and flexible and variable structures lead to the generation of some unique bulk phase material properties such as crystal, electronics, conductivity and other dimensions, which determine the properties of the oxide surface and thus the catalyst performance. Therefore, conducting research on perovskite-type oxide catalysts opens a new avenue for the development of earth-abundant and cost-efficient electrocatalysts with excellent HER activity.

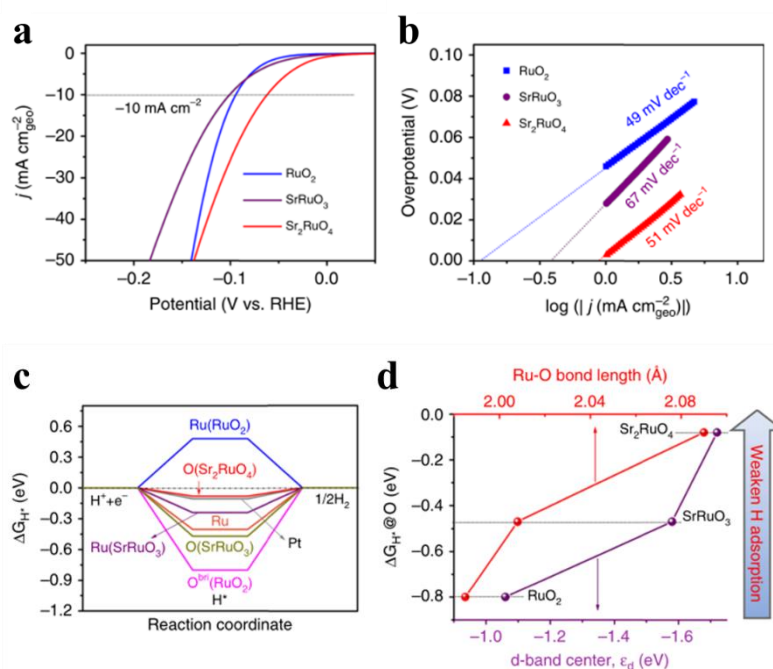


**Figure 5.** (a) Polarization curves and corresponding. (b) Tafel plots of  $\text{RuO}_2$ ,  $\text{SrRuO}_3$ , and  $\text{Sr}_2\text{RuO}_4$  catalysts in an Ar-saturated 1 M KOH solution. Scan rate,  $5 \text{ mV s}^{-1}$ . (c) Free-energy diagram for hydrogen adsorption at the metal and oxygen sites on  $\text{Sr}_2\text{RuO}_4$ ,  $\text{SrRuO}_3$ ,  $\text{RuO}_2$ , Ru, and Pt. (d) Relationship between  $\Delta G_{\text{H}^*@\text{O}}$  and d-band center as well as Ru-O bond length. Reproduced with permission [82]. Copyright 2019, Nature Publishing Group.

## 6. CONCLUSIONS

This paper summarizes some recent work progress on metal oxides in HER catalysis, including the catalyst preparation methods, testing methods and catalytic effects. And the recent research trends

also focus on heterostructures, and different materials such as metal/metal oxide, metal oxide/metal oxide, metal oxide/nonmetal substances (such as nitrogen, carbon, phosphorus, sulfur, etc.), and perovskite-type metal oxide have been prepared by different synthesis methods. The heterogeneous structure has a synergistic catalytic effect, especially in alkaline solutions, which can promote water cleavage and accelerate the Volmer step, thus affecting the catalytic effect.

Most metal oxides are more durable than metals, so enhancing the HER catalytic performance of metal oxides is a major task for researchers. The analysis of recent research literature shows that the factors affecting the catalytic effect of catalysts are mainly attributed to three aspects: (i) high specific surface area, (ii) oxygen vacancies, (iii) electrical conductivity. At this stage, most of the high-efficiency HER catalytic materials reach the nanoscale structure, and different treatments during the preparation of electrodes result in different surface structures. For example, nanosheet or nanorod (wire) array surface structures improve the specific surface area through defective sites formed in the material, or increase the number of edge active sites, thus effectively improving the catalytic activity. Appropriate surface structures can likewise improve the electron transport on the surface, which increases the electrical conductivity and thus the catalytic activity. In addition, the conductivity of metal oxides can also be improved by adding conductive agents such as carbon nanotubes CNT. Oxygen vacancies are an intrinsic defect in metal oxides, and a large number of oxygen vacancies in metal oxides can promote the adsorption of H<sub>2</sub>O in solution and lay the foundation for the next step of water dissociation and hydrogen desorption.

Furthermore, in addition to performing microscopic characterization and electrochemical testing experiments, the validation of theoretical studies is crucial. DFT calculations can be used to see how different catalyst surfaces affect HER catalysis and what relationships exist between the adsorption/desorption energies of water, protons and hydroxide ions, and how they affect the final reaction rate. The combination of experimental and theoretical calculations allows the use of different materials to reconcile different catalysts with high catalytic activity, thus overcoming the difficulty of large material screening. Although metal oxides have shown some success in the field of HER catalysis, there is still a huge scope for the preparation of efficient and stable catalysts.

## References

1. A. Midilli, M. Ay, I. Dincer and M. A. Rosen, *Renewable and sustainable energy reviews*, 9(2005)255-271.
2. T. N. Veziroğlu and S. Şahi, *Energy conversion and management*, 49(2008)1820-1831.
3. C.-J. Winter, *International journal of hydrogen energy*, 34(2009)S1-S52.
4. S. Dutta, *International Journal of Hydrogen Energy*, 15(1990)379-386.
5. M. Saxe and P. Alvfors, *Energy*, 32(2007)42-50.
6. S. Srinivasan and F. J. Salzano, *International Journal of Hydrogen Energy*, 2(1977)53-59.
7. J. Wang, F. Xu, H. Jin, Y. Chen and Y. Wang, *Adv Mater*, 29(2017)1605838.
8. J. K. Nørskov, T. Bligaard, A. Logadottir, J. R. Kitchin, J. G. Chen, S. Pandelov and U. Stimming, *Journal of The Electrochemical Society*, 152(2005)J23.
9. J. Greeley, T. F. Jaramillo, J. Bonde, I. B. Chorkendorff and J. K. Nørskov, *Nat Mater*, 5(2006)909-913.

10. E. Skúlason, V. Tripkovic, M. E. Björketun, S. Gudmundsdottir, G. Karlberg, J. Rossmeisl, T. Bligaard, H. Jónsson and J. K. Nørskov, *The Journal of Physical Chemistry C*, 114(2010)18182-18197.
11. J. Mahmood, F. Li, S.-M. Jung, M. S. Okyay, I. Ahmad, S.-J. Kim, N. Park, H. Y. Jeong and J.-B. Baek, *Nature Nanotechnology*, 12(2017)441-446.
12. M. Gong, W. Zhou, M. C. Tsai, J. Zhou, M. Guan, M. C. Lin, B. Zhang, Y. Hu, D. Y. Wang, J. Yang, S. J. Pennycook, B. J. Hwang and H. Dai, *Nat Commun*, 5(2014)4695.
13. J. Wei, M. Zhou, A. Long, Y. Xue, H. Liao, C. Wei and Z. J. Xu, *Nanomicro Lett*, 10(2018)75.
14. T. Ling, T. Zhang, B. Ge, L. Han, L. Zheng, F. Lin, Z. Xu, W. B. Hu, X. W. Du, K. Davey and S. Z. Qiao, *Adv Mater*, 31(2019)e1807771.
15. J. Lee, S. A. Sher Shah, P. J. Yoo and B. Lim, *Chemical Physics Letters*, 673(2017)89-92.
16. C. Cheng, S. S. A. Shah, T. Najam, X. Qi and Z. Wei, *Electrochimica Acta*, 260(2018)358-364.
17. L. Zhang, K. Xiong, S. Chen, L. Li, Z. Deng and Z. Wei, *Journal of Power Sources*, 274(2015)114-120.
18. K. Xiong, L. Li, Z. Deng, M. Xia, S. Chen, S. Tan, X. Peng, C. Duan and Z. Wei, *Rsc Advances*, 4(2014)20521.
19. S. Cherevko, S. Geiger, O. Kasian, A. Mingers and K. J. Mayrhofer, *Journal of Electroanalytical Chemistry*, 774(2016)102-110.
20. J. Ahmed and Y. Mao, *Electrochimica Acta*, 212(2016)686-693.
21. A. G. Vidales, L. Dam-Quang, A. Hong and S. Omanovic, *Electrochimica Acta*, 302(2019)198-206.
22. M. M. Ibrahim, A. Mezni, M. Alsawat, T. Kumeria, M. R. Das, S. Alzahly, A. Aldalbahi, K. Gornicka, J. Ryl and M. A. Amin, *International Journal of Energy Research*, 43(2019)5367-5383.
23. M. Gong, D.-Y. Wang, C.-C. Chen, B.-J. Hwang and H. Dai, *Nano Research*, 9(2015)28-46.
24. T. Ling, D. Y. Yan, H. Wang, Y. Jiao, Z. Hu, Y. Zheng, L. Zheng, J. Mao, H. Liu, X. W. Du, M. Jaroniec and S. Z. Qiao, *Nat Commun*, 8(2017)1509.
25. D. Soares, O. Teschke and I. Torriani, *Journal of The Electrochemical Society*, 1992, 139(9)98-105.
26. D. Soares, M. Kleinke, I. Torriani and O. Teschke, *International journal of hydrogen energy*, 19(1994)573-578.
27. X. Yan, L. Tian and X. Chen, *Journal of Power Sources*, 300(2015)336-343.
28. X. Liu, X. Wang, X. Yuan, W. Dong and F. Huang, *Journal of Materials Chemistry A*, 4(2016)167-172.
29. T. Zhang, M.-Y. Wu, D.-Y. Yan, J. Mao, H. Liu, W.-B. Hu, X.-W. Du, T. Ling and S.-Z. Qiao, *Nano Energy*, 43(2018)103-109.
30. K. Lu, Y. Liu, F. Lin, I. A. Cordova, S. Gao, B. Li, B. Peng, J. Kaelin, D. Coliz, C. Wang, Y. Shao and Y. Cheng, *J Am Chem Soc*, 142(2020)12613-12619.
31. X. Yan, L. Tian, M. He and X. Chen, *Nano Lett*, 15(2015)6015-6021.
32. H. Jin, J. Wang, D. Su, Z. Wei, Z. Pang and Y. Wang, *Journal of the American Chemical Society*, 137(2015)2688-2694.
33. X. Liu, C. Dong, W. Dong, X. Wang, X. Yuan and F. Huang, *RSC Advances*, 6(2016)38515-38520.
34. S. Saha, S. Chhetri, P. Khanra, P. Samanta, H. Koo, N. C. Murmu and T. Kuila, *Journal of Energy Storage*, 6(2016)22-31.
35. J. X. Feng, H. Xu, Y. T. Dong, X. F. Lu, Y. X. Tong and G. R. Li, *Angew Chem Int Ed Engl*, 56(2017)2960-2964.
36. N. Roy, K. T. Leung and D. Pradhan, *The Journal of Physical Chemistry C*, 119(2015)19117-19125.
37. S. Nong, W. Dong, J. Yin, B. Dong and F. Huang, *Journal of the American Chemical Society*, 140(2018)5719-5727.

38. S. P. Narayanan, P. Thakur, A. P. Balan, A. A. Abraham and M. R. Anantharamaniyer, *Physica Status Solidi Rapid Research Letters*, 13(2019)1900025.
39. Y. Rao, L.-M. Zhang, X. Shang, B. Dong, Y.-R. Liu, S.-S. Lu, J.-Q. Chi, Y.-M. Chai and C.-G. Liu, *Applied Surface Science*, 423(2017)1090-1096.
40. P. Jiang, Y. Yang, R. Shi, G. Xia, J. Chen, J. Su and Q. Chen, *Journal of Materials Chemistry A*, 5(2017)5475-5485.
41. G. H. Han, H. Kim, J. Kim, J. Kim, S. Y. Kim and S. H. Ahn, *Applied Catalysis B: Environmental*, 270(2020)118895.
42. Y. Jin and P. K. Shen, *Journal of Materials Chemistry A*, 3(2015)20080-20085.
43. R. D. Nikam, A. Y. Lu, P. A. Sonawane, U. R. Kumar, K. Yadav, L. J. Li and Y. T. Chen, *ACS Appl Mater Interfaces*, 7(2015)23328-23335.
44. X. Chen, G. Liu, W. Zheng, W. Feng, W. Cao, W. Hu and P. Hu, *Advanced Functional Materials*, 26(2016)8537-8544.
45. J. Zhang, T. Wang, P. Liu, Z. Liao, S. Liu, X. Zhuang, M. Chen, E. Zschech and X. Feng, *Nat Commun*, 8(2017)15437.
46. Y. Liu, B. Huang and Z. Xie, *Applied Surface Science*, 427(2018)693-701.
47. C. Jian, Q. Cai, W. Hong, J. Li and W. Liu, *Small*, 14(2018)e1703798.
48. H. Hu, M. Tian, F. Li, L. Gao, N. Xu, Y. Hu, X. Long, J. Ma and J. Jin, *Chemelectrochem*, 5(2018)2660-2665.
49. X. Li, J. Yu, J. Jia, A. Wang, L. Zhao, T. Xiong, H. Liu and W. Zhou, *Nano Energy*, 62(2019)127-135.
50. X. Liu, K. Ni, C. Niu, R. Guo, W. Xi, Z. Wang, J. Meng, J. Li, Y. Zhu, P. Wu, Q. Li, J. Luo, X. Wu and L. Mai, *ACS Catalysis*, 9(2019)2275-2285.
51. A. Bonakdarpour, R. T. Tucker, M. D. Fleischauer, N. A. Beckers, M. J. Brett and D. P. Wilkinson, *Electrochimica Acta*, 85(2012)492-500.
52. Y. Li, J. Zhang, X. Qian, Y. Zhang, Y. Wang, R. Hu, C. Yao and J. Zhu, *Applied Surface Science*, 427(2018)884-889.
53. M. Kaur and K. Pal, *International Journal of Hydrogen Energy*, 41(2016)21861-21869.
54. J. F. Gao, Y. Y. Gao, C. H. Tan, L. I. Ye-Ping, J. Guo and S. Y. Zhang, *Fine Chemicals*, 29(2012)4.
55. J. G. S. Moo, Z. Awaludin, T. Okajima and T. Ohsaka, *Journal of Solid State Electrochemistry*, 17(2013)3115-3123.
56. Z. Awaludin, T. Okajima and T. Ohsaka, *Chemistry Letters*, 43(2014)1248-1250.
57. H. Yan, C. Tian, L. Wang, A. Wu, M. Meng, L. Zhao and H. Fu, *Angewandte Chemie International Edition*, 54(2015)6325-6329.
58. L. Yang, X. Zhu, S. Xiong, X. Wu, Y. Shan and P. K. Chu, *ACS Appl Mater Interfaces*, 8(2016)13966-13972.
59. S. M. A. Shibli, V. R. Anupama, P. S. Arun, P. Jineesh and L. Suji, *International Journal of Hydrogen Energy*, 41(2016)10090-10102.
60. Y. L. Kim, H. A. Choi, N. S. Lee, B. Son, H. J. Kim, J. M. Baik, Y. Lee, C. Lee and M. H. Kim, *Phys Chem Chem Phys*, 17(2015)7435-7442.
61. Q. Feng, M. Li, T. Wang, Y. Chen, X. Wang, X. Zhang, X. Li, Z. Yang, L. Feng, J. Zheng, H. Xu, T. Zhai and Y. Jiang, *Applied Catalysis B: Environmental*, 271(2020)118924.
62. T. D. Nguyen, D. Mrabet and T. O. Do, *Journal of Physical Chemistry C*, 112(2008)15226-15235.
63. W. C. Chueh, C. Falter, M. Abbott, D. Scipio, P. Furler, S. M. Haile and A. Steinfeld, *Science*, 330(2015)1797-1801.
64. Z. Chen, G. Shao, Z. Ma, J. Song, G. Wang and W. Huang, *Materials Letters*, 160(2015)34-37.
65. K. Zhang, J. Li, W. Liu, J. Liu and C. Yan, *International Journal of Hydrogen Energy*, 41(2016)22643-22651.

66. A. R. Madram, M. Mohebbi, M. Nasiri and M. R. Sovizi, *Iranian Journal of Hydrogen & Fuel Cell*, 5(2018)1-11.
67. S. M. A. Shibli, L. Thushara and S. R. Archana, *International Journal of Hydrogen Energy*, 42(2017)1919-1931.
68. S. M. A. Shibli, A. H. Riyas, M. Ameen Sha and R. Mole, *Journal of Alloys and Compounds*, 696(2017)595-603.
69. S. M. A. Shibli and M. Ameen Sha, *Journal of Alloys and Compounds*, 749(2018)250-261.
70. Z. Weng, W. Liu, L. C. Yin, R. Fang, M. Li, E. I. Altman, Q. Fan, F. Li, H. M. Cheng and H. Wang, *Nano Lett*, 15(2015)7704-7710.
71. H. Liu, S. Zeng, P. He, F. Dong, M. He, Y. Zhang, S. Wang, C. Li, M. Liu and L. Jia, *Electrochimica Acta*, 299(2019)405-414.
72. X. Yi, P. He, Y. Chen, W. Wang, D. Yang and F. Dong, *Electrochemical Technologies for Hydrogen Production*, 28(2010)13-20.
73. S. Voskanyan, A. Tzanev, N. Shroti, G. Pchelarov and K. Petrov, *Izvestiya Po Khimiya Bulgarska Akademiya Na Naukite*, 48(2016)84-91.
74. P. He, X. Yi, Y. Ma, W. Wang, F. Dong, L. Du and H. Liu, *Journal of Physics and Chemistry of Solids*, 72(2011)1261-1264.
75. L. C. Seitz, C. F. Dickens, K. Nishio, Y. Hikita, J. Montoya, A. Doyle, C. Kirk, A. Vojvodic, H. Y. Hwang and J. K. Nørskov, *Science*, 353(2016)1011-1014.
76. Y. Zhu, W. Zhou and Z. Shao, *Small*, 13(2017)1603793.
77. J. Hwang, R. R. Rao, L. Giordano, Y. Katayama, Y. Yu and Y. Shao-Horn, *Science*, 358(2017)751-756.
78. X. Xu, Y. Chen, W. Zhou, Z. Zhu, C. Su, M. Liu and Z. Shao, *Adv Mater*, 28(2016)6442-6448.
79. Z. Zhang, Y. Chen, Z. Dai, S. Tan and D. Chen, *Electrochimica Acta*, 312(2019)128-136.
80. Q. Sun, Z. Dai, Z. Zhang, Z. Chen, H. Lin, Y. Gao and D. Chen, *Journal of Power Sources*, 427(2019)194-200.
81. Y. Sugawara, K. Kamata and T. Yamaguchi, *ACS Applied Energy Materials*, 2(2019)956-960.
82. Y. Zhu, H. A. Tahini, Z. Hu, J. Dai, Y. Chen, H. Sun, W. Zhou, M. Liu, S. C. Smith, H. Wang and Z. Shao, *Nature Communications*, 10(2019)1-9.
83. D. Guan, J. Zhou, Y. C. Huang, C. L. Dong, J. Q. Wang, W. Zhou and Z. Shao, *Nat Commun*, 10(2019)3755.